Pd^{II} and Pt^{II} Complexes with a Thio-Aza Macrocycle Ligand Containing an Intercalating Fragment: Structural and Antitumor Activity Studies

Stefano Amatori,[a] Gianluca Ambrosi,[b] Alfredo Errico Provenzano,[a,‡] Mirco Fanelli,[a,*] Mauro Formica,[b] Vieri Fusi,[b,*] Luca Giorgi,[b] Eleonora Macedi,[c] Mauro Micheloni,[b] Paola Paoli,[c,‡] and Patrizia Rossi[c]

[a] *University of Urbino, Molecular Pathology Lab. "PaoLa", Department of Biomolecular Sciences, Arco d'Augusto 2, I-61032 Fano (PU), Italy.* [b] *University of Urbino, Department of Pure and Applied Sciences, Via della Stazione 4, I-61029 Urbino, Italy.* [c] *University of Firenze, Department of Industrial Engineering, Via S. Marta 3, I-50139 Firenze, Italy.*

[*] Corresponding Authors:

Prof. V. Fusi, E-mail: vieri.fusi@uniurb.it; Fax: +39 0722.350032; Tel: +39 0722.304882

Prof. M. Fanelli, E-mail: mirco.fanelli@uniurb.it; Fax: +39 0722.304970; Tel: +39 0722.304951

[‡] These authors contributed equally.

Abstract

Two new Pt^{II} and Pd^{II} complexes of formula [**L**MCl_2] (M = Pt, Pd) were synthesized and characterized both in solution and solid state. They were obtained using the thio-aza macrocycle 9,18-dimethyl-12,17dithio-9,18,27,28-tetraaaza-29-oxatetracyclo[24.2.1.$0^{2,7}$.$0^{20,25}$]enneicosa-2,4,6,20,22,24,26,28^{1}-octaene (**L**) containing the 2,5-diphenyl[1,3,4]oxadiazole as intercalating fragment. M^{II} is coordinated in *cis*-position by the two S atoms of **L**. The two crystal structures of [**L**$PtCl_2$] and [**L**$PdCl_2$] complexes showed that the M^{II} ion is located outside the macrocyclic cavity. The square planar coordination sphere fulfilled by two chloride anions in a cisplatin-like arrangement with the chloride leaving groups exposed to the environment. The biological activity of both [**L**$PtCl_2$] and [**L**$PdCl_2$], monitored towards a leukemic cellular model (U937), is coherent with their ability to interfere, at different levels, with the DNA structure.

Keywords: Platinum complexes / Palladium complexes / Macrocycle / Antineoplastic drugs / Cancer

Introduction

Cancer is one of the main causes of morbidity and mortality worldwide, with approximately 14 million new cases and 8.2 million cancer related deaths reported in 2012, thus affecting life expectancy and producing a negative impact on society [1]. In this light, there is a continuous request of new improved anticancer drugs; the discovery of cisplatin (*cis*-$Pt(NH_3)_2Cl_2$) has fostered the research on metal complexes in order to obtain new molecules characterized by improved biological activities, in terms of cellular selectivity and therapeutic efficiency, while minimizing their side effects [2-9]. The pharmaceutical industry is investing enormous amount

of money in new metal-based drugs trying to overcome the side effects connected with the use of cisplatin such as, emesis, renal toxicity, bone marrow suppression, neurotoxicity, hearing loss and drug resistance [10,11]. The economic interest in metal-based drugs is attested by the appearance of more than sixty patents in the period 2013-2015 only concerning platinum complexes for tumor treatments.

The rationale in the design of cisplatin analogues comes both from the results of the mechanistic investigations and simple coordination chemistry considerations. The general topology consists in a coordinated neutral square planar complex featuring two leaving groups in *cis*-position (chlorides and carboxylates are the most commons) and the other two positions occupied by two monodentate or one bidentate carrier ligands usually containing N-amine as the binding atom. It is to remember that once within the cell one or both leaving groups are replaced by water molecules; the resulting adduct should be quite stable from the kinetic point of view because N-ligands have a low *trans*-effect [12] (another parameter that must be taken into account in the design of new cisplatin analogues). Due to the *cis* geometry of the metal complex, 1,2-intrastrand crosslinks form between adjacent guanines (60-65%, 20-25% between adjacent adenines and guanines) as well as 1,3-intrastrand crosslinks (due to geometric reason, the *trans* isomer cannot form this kind of crosslinks). The resulting intrastrand adduct, which makes DNA distort and bend, causes different cellular responses, such as transcription inhibition, replication and cell-cycle arrest, DNA repair and apoptosis [4].

The research on metal complexes other than the Pt^{II} ones is constantly growing up and many metal ions, mainly belonging to the class of noble metals, have been studied with this aim [13]. Among them, the interest towards the Pd^{II} is increasing because, belonging it to the same group of Pt^{II}, it forms complexes of similar geometry. Pd^{II} complexes show different kinetic and

thermodynamic stability of both main ligand and leaving groups. They are usually thermodynamically less stable and kinetically more reactive (about 10^5 times) than the corresponding Pt^{II} analogues [13,14], leading an easier and faster substitution of its coordination positions. Moreover, the better solubility compared to platinum complexes, makes Pd^{II} attractive in the field. In addition, Pd^{II} preferentially forms *trans* complexes thus leading, at least at the beginning, to inactive species; for this reason, a bidentate chelating ligand would be preferable to overcome this drawback.

Typical ligands in the field show two N amine functions as M^{II} coordinating groups while those containing S have been scarcely investigated although they should form kinetically stable complexes with the soft Pt^{II} and Pd^{II} cations. The main ligands containing S as donor atom belong to dithiocarbamate and thiosemicarbazone classes [15-23] while the thioethers are scarcely investigated. In the case, the *trans*-effect, responsible to labialize the ligand bound in *trans*-position to S more than that to N, could modulate the interaction with the DNA in a different and efficient way [14].

Metal systems can interact with DNA also by non-covalent interactions being the most important the π-π stacking interactions, commonly observed between two aromatic groups. They give rise to the intercalating binding mode resulting from the insertion of an aromatic ring belonging to the metal-system between base pairs of the DNA double helix [24-29].

Following the idea to have kinetically stable complexes that can draw up metal complex and DNA, aromatic fragments capable of intercalation into DNA, such as phenanthroline [30,31], bipyridyl [32,33] and many others [25,28,32-38], have been inserted in the ligand to favour the metal-complex activity [5].

Considering the whole ligand, those based on a macrocyclic topology are rare due to their ability to saturate the coordination requirement of the metal ion.

Herein we report the use of the dithio-diaza-macrocyclic ligand **L** (Figure 1) in which the 2,5-diphenyl[1,3,4]oxadiazole (PPD) fragment has been inserted in the framework [39].

The ligand shows binding sites suitable to stabilize Pt^{II} and Pd^{II} ions, that are two thioether functions, and the intercalating PPD fragment. Indeed, the thioether ethylenic chain can bind Pt^{II} and Pd^{II} to afford a structurally cisplatin-like topology while the PPD fragment could facilitate the interaction with DNA by intercalation, thus inserting a new variable in these potential antitumor drugs.

The solution and solid state characterization of the Pt^{II} and Pd^{II} complexes and their biological activity against a cancer cellular model (U937) have been reported. Furthermore, the possible mechanism of action was investigated through cell-free experimental approaches able to dissect the reversible and irreversible phenomena that involve the DNA structure.

Experimental

Synthesis

All chemicals were purchased from Aldrich in the highest quality commercially available. All the solvents were dried prior to use. Ligand 9,12-Dimethyl-9,12,27,28-tetraaza-15,18-dithia-29-oxatetracyclo[24.2.1.$0^{2,7}$.$0^{20,25}$]-enneicosa-2,4,6,20,22,24,26,28^{1}-octaene (**L**) was prepared as already described [39].

[$LPdCl_2$]

Ligand **L** (45 mg, 0.10 mmol) and potassium tetrachloropalladate (K_2PdCl_4, 33 mg, 0.10 mmol) were dissolved in dry DMF (5 mL) and stirred at 60 °C for 30 min. The solution was kept at room temperature overnight obtaining the complex as an orange microcrystalline precipitate. The solid was filtered and washed with ethanol to remove any trace of DMF affording 47 mg of pure complex (yield 74 % with respect to **L**). MS-ESI: m/z=631.0 (M+H). Elem Anal (%) calcd for $C_{24}H_{30}Cl_2N_4OPdS_2$: C, 45.61; H, 4.78; N, 8.87; found: C, 45.6; H, 4.9; N, 8.9.

Crystals suitable for X-ray analysis have been obtained by slow evaporation of a more diluted DMF solution of [**L**$PdCl_2$] complex.

[LPtCl$_2$]·0.5DMF

Ligand **L** (45 mg, 0.10 mmol) and potassium tetrachloroplatinate (K_2PtCl_4, 42 mg, 0.10 mmol) were dissolved in dry DMF (5 mL) and stirred at 60 °C for 30 min. The solution was kept at room temperature overnight obtaining the complex as a light yellow microcrystalline precipitate. The solid was filtered and washed with ethanol to remove any trace of DMF affording 57 mg of pure complex (yield 72 % with respect to **L**). MS-ESI: m/z=719.1 (M+H). Elem Anal (%) calcd for $C_{24}H_{30}Cl_2N_4OPdS_2{\cdot}0.5(C_3H_7NO)$: C, 40.45; H, 4.46; N, 8.32; found: C, 40.5; H, 4.4; N, 8.2.

Crystals suitable for X-ray analysis have been obtained by slow evaporation of a more diluted DMF solution containing complex [**L**$PtCl_2$]·0.5DMF.

X-ray crystallography

Intensity data for compounds [**L**$PdCl_2$] and [**L**$PtCl_2$]·0.5(DMF) were collected on an Oxford Diffraction Xcalibur diffractometer using a Mo-K_α radiation (λ = 0.71073 Å). Data collection and reduction were performed with the program CrysAlisPro [40]; absorption correction was

performed with the SCALE3 ABSPACK scaling algorithm in CrysAlisPro [40]. The structures were solved by using the SIR-97 [41] package and subsequently refined on the F^2 values by the full-matrix least-squares program SHELXL-97 [42]. In both structures, the non-hydrogen atoms were anisotropically refined. In [**L**$PdCl_2$] the hydrogen atoms were found in the difference Fourier map and freely refined with isotropic temperature factors, while in [**L**$PtCl_2$]·0.5(DMF) they were put in calculated positions and isotropically refined accordingly to the bound atom. The DMF molecule is affected by some disorder and an occupancy factor of 0.5 was assigned. Table 2 reports crystallographic and refinement details.

Geometrical calculations were performed by PARST97 [43] and molecular plots were produced by the Mercury 2.4 [44] and the ORTEP3 [45] programs.

NMR Experimental Methods

The ^1H and ^{13}C spectra were recorded on a Bruker Avance 400 spectrometer, operating at 400.13 and 100.61 MHz, respectively equipped with a PABBO Z-gradients direct probe and a variable temperature unit. ^1H and ^{13}C NMR spectra are referenced to residual solvent signals. The assignment of the NMR resonances was supported by 135-DEPT and 2D experiments. Two-dimensional experiments (COSY, NOESY and HMQC) were recorded using standard Bruker pulse sequences. The 2D-NOESY experiments were recorded using a mixing time (d8) of 0.35 s. ^1H NMR titrations were carried out in a DMF-d_7-5% D_2O mixture. ^1H-NMR titration experiments were carried out at 298 K by the addition of K_2PtCl_4 or K_2PdCl_4 (7.0×10^{-5} mmol/µL) to ligand **L** (5.3×10^{-3} mmol/0.6 mL in *N*,*N*-Dimethylformamide-d_7). The tube was then kept for 2h before starting the acquisition of the spectrum; further waiting time up two days did not afford variation of spectra.

Fluorimetric assay

DNA (60 ng) was incubated for 90 min at 37 °C with increasing concentrations (0.5-1-2-3-4 mM) of each compound, in a final volume of 10 μl of 10 mM Tris-HCl buffer (pH 7.4) and then stained for 3 min with Quant-iT™ PicoGreen® dsDNA Assay Kit® following the manufacturer's instructions (Life Technologies). Sample fluorescence was measured on a Qubit® 2.0 Fluorometer (Life Technologies). Values are reported as mean ± SD of five independent experiments.

DNA electrophoretic mobility assay

An amount of 500 ng of pLL3.7 plasmid DNA was incubated for 90 min (in dose-response experiments) at 37 °C with the compounds (at the reported concentrations) in a final volume of 20 μl of 10 mM Tris-HCl buffer (pH 7.4). After incubation, DNA was separated by 0.8% agarose gel electrophoresis (AGE) in presence or not of ethidium bromide (Et-Br). At the end of AGE, the gels were incubated with Et-Br staining solution (0.5 μg/ml in 1xTAE) for 30 min at room temperature.

Biological activity

Immortalized promonocytic leukaemia (U937) cell line was obtained from American Type Culture Collection (ATCC). Cells were grown in RPMI 1640 (Lonza) supplemented with 10% foetal bovine serum, 1% penicillin-streptomycin and 1% glutamine in a humidified atmosphere at 37 °C as previously described [46]. Cisplatin (cis-Pt) was dissolved at 8 mM in distilled water while all the other compounds were dissolved at 10 mM in Dimethylformamide (DMF) as stock

solutions, stored at -80 °C and subsequently diluted before use. Treatments were carried out at the concentrations reported in the figures and cellular viability was evaluated, after 24 h of treatment, by both Trypan blue dye exclusion assay (using TC10 automatic cell counter – Bio-Rad) and XTT assay (using Benchmarck microplate reader – Bio-Rad) . The 50% inhibitory concentration (IC_{50}) values were calculated with CompuSyn software (ComboSyn, Inc.) [47]. The data are reported as mean (± SD) resulting from three independent experiments.

Cell cycle profile and percentage of hypodiploid cells were studied by propidium iodide staining procedure as previously reported [48]. Briefly, U937 cells were fixed in ice-cold 70% ethanol and stained using a propidium iodide staining solution (50 μg/ml). Cytofluorimetric acquisitions were carried out with a PAS flow cytometer (Partec) and sample analysis was carried out with FlowJo 8.6.3 software (Tree Star, Inc.). Cell cycle per cent values were calculated using the Dean/Jett/Fox model.

Results and Discussion

Synthesis of the complexes

The Pt^{II}-**L** and Pd^{II}-**L** complexes were synthesized and characterized both in solution and solid state. Both solid complexes have been obtained in high yield by simple mixing **L** and the corresponding tetrachloride potassium salt in DMF solution. The DMF solution was kept warm to avoid the precipitation of **L**, due to its scarce solubility in cold DMF, thus allowing the formation of the complexes. Complexes precipitated as microcrystalline solids, were stable in air and do not need any further purification. The solid compounds resulted neutral complexes of [**L**MCl_2] formula (M = Pt^{II} or Pd^{II}).

NMR Studies

NMR solution studies were performed in dimethylformamide (DMF-5% water) to highlight the binding function involved in the species present in solution. Figure 2 reports the ^{1}H NMR spectra of **L**, [**L**$PtCl_2$] and [**L**$PdCl_2$] species; it clearly shows that the binding of M^{II} affects the NMR resonances of **L** with both metal ions. The [**L**MCl_2] species is also soluble in CD_3CN and dimethyl sulfoxide (DMSO-d_6) obtaining similar NMR spectra and, in the case of DMSO, without destroying the complex. This latter observation suggests that **L** forms stable complexes with both Pt^{II} and Pd^{II} ions because their de-coordination in DMSO was not observed as it often occurs in many complexes due to the high affinity of DMSO for such metal ions. The pattern of resonances of the [**L**$PtCl_2$] and [**L**$PdCl_2$] species (Figure 2) resulted similar both in signals and chemical shifts; only a different resolution of the signals, broader for [**L**$PdCl_2$] than for [**L**$PtCl_2$], can be observed. This occurred in all solvents investigated, suggesting a similar coordination environment in solution and a similar conformational stability of the formed species.

NMR titration experiments exhibited similar final spectra to those recorded dissolving the solid complexes for both metal ions also highlighting that the [**L**MCl_2] species are fully formed after the addition of one equivalent of M^{II} ion (see Supplementary Information, Figures S1, S2); this suggests the high stability of such species. The analysis of the NMR spectra showed the simultaneous presence of two different Pt^{II} and Pd^{II} species in solution slowly exchanging on the NMR time scale (Figure 2). Both species, named **a** and **b** in Figure 2, show the same C_s symmetry on the NMR time scale as confirmed by ^{13}C NMR spectra which exhibited twelve resonances for each species excluding an unsymmetrical coordination environment (Supplementary Information, Figures S3). The two **a** and **b** species, although similar to each other in the Pt^{II} and Pd^{II} complexes, are present in small different percentage (**a**=70% **b**=30% for

[**L**$PtCl_2$] and **a**=80% **b**=20% for [**L**$PdCl_2$]). The two patterns of signals started to collapse in only one broad pattern at T > 373 K (data not shown), supporting the presence of two conformers slowly exchanging on the NMR time scale. The attribution of all resonances has been possible by using ^{1}H-^{1}H and ^{1}H-^{13}C NMR correlation experiments as that reported in Figure S4 for the [**L**$PtCl_2$] species. Comparing the ^{1}H NMR spectra of free **L** and [**L**$PtCl_2$] species, the binding of Pt^{II} produced more ^{1}H NMR signals with respect to free **L** for both **a** and **b** species. This can be attributed to the stiffening of the macrocyclic ring as often observed in macrocyclic metal complexes [49,50]. In this case, it removes the equivalence of the protons belonging to the same methylene group but not between the same groups. In fact, the ethylene chain linking the two S atoms gave rise to a singlet (H1) in the ^{1}H NMR spectrum of free **L** but to a more complex pattern of signals for **a** and **b** species (Figure 2); however, all H1 resonances correlated to only one carbon atom of the ^{13}C NMR spectrum (Figure S4) which exhibited only one signal for this chain in free and complexed **a** and **b** species. Similar considerations can be done for the resonances of H2, H3 and H5 (see below) as well as for the methyl group H4 exhibiting only one singlet for each **a** and **b** species in both ^{1}H and ^{13}C NMR spectra. All these signals are in agreement with a C_s symmetry for the species on the NMR time scale. Examining the shift of the signals in the ^{1}H NMR experiments, the resonances H1 and H2, belonging to the methylene groups in α-position to a S atom, exhibited the higher downfield shift with respect to free **L** in both **a** and **b** species. On the contrary, H3 and H4, belonging to the methylene and methyl group, respectively, in α-position to the amine functions, exhibited a smaller (H3) or an unappreciable (H4) downfield shift. The aromatic PPD resonances are slightly perturbed by the Pt^{II} coordination while the H5 resonances belonging to the methylene chain linking PPD and amine functions, merit a short discussion. Considering the **a** and **b** species, as above mentioned, the

equivalence of the two H5 protons into the same group was removed by the insertion of the metal ion. They pass from a singlet in **L** to two doublets due to an AB system, (*J*=13.0 Hz) in each **a** and **b** species preserving the same equivalence between the two groups (only two doublets in the ^{1}H and one signal in the ^{13}C NMR spectra for each species), on the NMR time scale. The signals of the two unequivalent H5 protons in **a** exhibited higher down and up field shift than those of **b** species although, considering the average of the shift, they resonanced at similar chemical shift of free **L** in both **a** and **b** complexes. The stiffening of the molecule due to the coordination of the metal ion removes, as above, the NMR equivalence of the two methylene protons H5 in both species. In the **a** species, the large opposite shift can be justified by the different spatial positions of the two H5 protons with respect to the PPD rings; the two protons are probably located in a different position with respect to the anisotropic cone of the aromatic ring undergoing to an opposite shift. Overall, the higher downfield shift exhibited by H1 and H2 together with the scarce shift of H3, H4 and PPD resonances support that only the two thioether functions are involved in the Pt^{II} coordination. Similar considerations can be made for the [**L**$PdCl_2$] species. This hypothesis is also supported by UV-Vis and fluorescence investigations where the addition of Pt^{II} and Pd^{II} metal ions did not affect the spectral profile of free **L** both in absorption and in emission (data not shown). In fact, it was demonstrated that the involvement of the amine function in metal ion coordination produced the increase of the fluorescent emission also for heavy metal ions such as Pb^{II} and Hg^{II}, due to the interruption of the PET effect from the amine lone pair to PPD moiety [39]; the absence of this effect suggests that the amine functions are not involved in the coordination of Pt^{II} and Pd^{II} ions.

Crystal Structures

The asymmetric unit of [**L**$PtCl_2$] contains one platinum complex and half molecule of DMF, while in the asymmetric unit of [**L**$PdCl_2$] only the palladium complex is present.

In both compounds the macrocycle **L** acts as a bidentate chelating ligand interacting with the metal cation through the two sulfur donors, as suggested in solution by NMR studies. In both crystal structures, as already observed in most of the metal complexes of noble ions with thiacrowns [51], the metal ion is not included in the ligand cavity: the S donor atoms are *exo* oriented, while the *endo* oriented N atoms are unbound. The coordination sphere of each metal cation is completed by two chlorine atoms and can be described as a planar square with the sulphur atoms *cis* arranged (Figure 3), being bond distances and angles (Table 1) within the expected range (Cambridge Structural Database, CSD, v. 5.35 data) [52]. As a result the metal complexes have very similar overall shapes (Figure 4). As a consequence of the *cis* arrangement of the sulphur donors, the SCH_2CH_2S moiety adopts a *gauche* conformation [60.1(2)° and 58.9(5)° for [**L**$PdCl_2$] and [**L**$PtCl_2$], respectively] and due to the *exo* coordination of the metal ion, the ethylene bridge points inside the macrocyclic cavity and, maybe more importantly, the chlorine atoms are exposed to the environment (*see below*). Therefore they could be promptly replaced by two water molecules upon entering the cell, thus becoming aquated (the first step in the mechanism of action of all platinum containing anticancer agents) [53]. Finally, each metal ion is well in the mean plane defined by the four donors (deviations are 0.0140(2) and 0.0101(3) Å for Pd and Pt, respectively) and, in both cases, the MCl_2S_2 moiety sits just above one of the aromatic rings of the ligand even if considerably remote from the C_6 centroid (4.5 and 4.2 Å for [**L**$PdCl_2$] and [**L**$PtCl_2$], respectively, with the M-C_6 centroid line almost perpendicular to the phenyl ring). In both cases, the PPD moiety takes a *transoid* conformation, that is, the side arms in the phenyl *ortho* positions point in opposite directions (Scheme 1). In fact, at least in principle,

the PPD moiety may adopt three different possible conformations (see Scheme 1): the *cisoid I* with both the side arms in the phenyl *ortho* positions oriented in the direction of the oxadiazole oxygen; the *cisoid II* form where both the side arms are oriented in the direction of the nitrogen atoms of the oxadiazole ring, and finally the already mentioned *transoid* conformation [54].

On the other hand, a survey of the solid state structures deposited in the CSD, featuring the molecular fragment sketched in Scheme 1 (see Supplementary Information), shows that the *cisoid II* conformation is the most common.

Interestingly, the parent compound having a N_4 set of donors *vs* N_2S_2 shows a *cisoid I* conformation in the copper and zinc complexes [55]. In that case the three rings are well in a plane, while in the N_2S_2 parent complexes the angles formed by each phenyl mean plane with the heterocycle are 15.1(1)/11.3(1)° and 7.4(2)/33.0(2)° for [**L**$PdCl_2$] and [**L**$PtCl_2$], respectively.

As a consequence of the *transoid* conformation, the adduct takes a cage-like overall shape with one of the phenyl rings pointing outside the molecular cavity and exposed to the surroundings (*see below*). Therefore, we can speculate that it could lie in a favourable position for a first non-covalent approach *via* π-π interactions with the DNA moiety. This observation is somehow supported by the fact that in the crystal lattice of the Pt(II) complex the exposed phenyl rings of two symmetry related complexes (2-x, -y, 1-z) appear weakly interacting via π-π contacts (the distance between their centroid is about 4 Å, see Supplementary Information Figure S5). As for the palladium species, the equivalent phenyl ring is involved in weak CH···π interactions with the hydrogen atom of a methylene group ($C_{6centroid}$···H distance ca. 3 Å, $C_{6centroid}$···H-C angle ca. 120°, see Supplementary Information Figure S6) of a symmetry related complex (1-x, 2-y, 1-z). In addition, both the crystal structures offer indirect hints about the exposure of the chlorine atoms to the environment (in view of their replacement by the water molecules once in the cell) through

their involvement in intermolecular contacts. In the platinum complex each chlorine atom weakly interacts with a different symmetry related complex via CH···Cl contacts: $C2^{i}\cdots Cl2$ 3.662(6) Å (i=1-x, 2-y,-z) and $C5^{ii}\cdots Cl1$ 3.809(7) Å (ii= 1-x, 1-y,-z, see Supplementary Information, Figure S5); while in the parent [**L**$PdCl_2$] compound one chlorine atom acts as bidentate acceptor towards two CH donors provided by two different metal complexes: $C11^{iii}\cdots Cl2$ 3.657(3) Å (iii=x, -1+y,-1+z) and $C5^{iv}\cdots Cl2$ 3.651(4) Å (iv= 2-x, 2-y,-z, see Supplementary Information, Figure S6). Finally, in both cases centrosymmetric dimers are formed through $CH\cdots N_{oxadiazole}$ weak contacts: $C23^{v}\cdots N3$ 3.685(9) Å and $C3^{v}\cdots N2$ 3.687(9) Å (v=1-x, 1-y, 1-z, see Supplementary Information, Figure S5) for [**L**$PtCl_2$]·0.5(DMF); $C23^{vi}\cdots N3$ 3.512(4) Å and $C2^{vi}\cdots N3$ 3.696(3) Å, (vi=2-x, 2-y, 1-z, see Supplementary Information, Figure S6) for ([**L**$PdCl_2$].

Biological Studies

The potential ability to intercalate in the DNA structure has been tested by a fluorimetric assay (Figure 5). The preincubation of DNA with [**L**$PtCl_2$] and [**L**$PdCl_2$] interferes with the subsequent intercalating ability of a fluorescent dye (PicoGreen - PG) in a concentration-dependent manner. The DNA staining interference was not monitored when the assay was conducted avoiding preincubation, but in presence of [**L**$PtCl_2$] or [**L**$PdCl_2$], thus excluding the possibility of dye quenching mediated by the compounds under investigation (data not shown). Interestingly, small fluctuations of the fluorescence were also observed when **L** or *cis*-Pt was used in the assay. However, the phenomenon appeared to be not dose-dependent and may be due, for **L**, to its possible intercalating ability and, for cisplatin, to the covalent modifications induced in the DNA structure [56].

In order to identify which properties of the molecules were responsible for the diminished staining of DNA, both [**L**$PtCl_2$] and [**L**$PdCl_2$] were incubated with plasmid DNA, that was subsequently subjected to electrophoretic separation in presence or in absence of the intercalating agent ethidium bromide (Et-Br, Figure 6): modifications of DNA attributable to the intercalating properties of the complexes can be reverted by the presence of the Et-Br during the electrophoretic separation of DNA itself. Notably, in absence of Et-Br, both [**L**$PtCl_2$] and [**L**$PdCl_2$] were able to induce a perturbation of the electrophoretic migration of plasmid DNA, at a concentration up to 2 mM (upper panels); this phenomenon was instead not detectable when the electrophoretic migration was conducted in presence of Et-Br (lower panels). Moreover, **L** was only able to slightly change the ratio between the two plasmid species (indicated by arrows, Figure 6) in accordance with the fluctuation monitored in the fluorimetric assay (Figure 5). Conversely, *cis*-Pt induced the well-known changes of mobility due to its ability to covalently modify the DNA through the generation of intra- and inter-strand covalent adducts [56].

Furthermore, incubations with high concentrations (2mM and 4mM) of either [**L**$PtCl_2$] or [**L**$PdCl_2$] are associated with a progressive decrease of DNA staining leading to the hypothesis of the induction of DNA degradation (Figure 6 and Supplementary Information, Figure S7). In order to investigate this phenomenon, the electrophoretic migration of the DNA was conducted with the linearized form of the plasmid after incubation with the compounds of interest. The electrophoretic assay showed a dose-dependent degradation of DNA with the appearance of the canonical DNA smear (Figure 7).

Finally, the study of the biological activity showed that both complexes were able to reduce the cell survival of leukemic (U937) cells (by trypan blue dye exclusion assay IC_{50} = 56.7 ± 3.2 μM and 55.3 ± 2.4 μM for [**L**$PtCl_2$] and [**L**$PdCl_2$], respectively - Figure 8). Moreover, we obtained a

comparable biological response by XTT assay (Supplementary Information, Figure S8). In addition, [**L**$PdCl_2$] induced an accumulation of cells in G1 phase of the cell cycle (similarly to **L**) but only [**L**$PtCl_2$] was able, at the same concentrations, to strongly perturb the cell cycle starting from an accumulation in G1 at low concentration (30 μM) to a complete altered cell cycle profile at higher concentration (50 μM, see Supplementary Information, Figure S9).

Moreover, both [**L**$PtCl_2$] and [**L**$PdCl_2$] induced an increased percentage of hypodiploid cells ([**L**$PdCl_2$] at high concentration while [**L**$PtCl_2$] also at low concentration) suggesting the involvement of the programmed cell death (Supplementary Information, Figure S10).

Conclusions

In summary, two Pt^{II} and Pd^{II} complexes were obtained using a macrocyclic ligand; due to their soft nature the metals prefer to be coordinated by the two thioether functions, as a consequence they are exposed to the environment in a *cis*-platinum like conformation. In addition, the presence in the ligand of the DNA-intercalating PPD fragment offers further interacting points for antineoplastic applications.

[**L**$PdCl_2$] and [**L**$PtCl_2$] demonstrated to exert biological activity against cancer cells such as decrease of cell survival, alteration of cell cycle profile and induction of cellular hypodiploidy. These phenomena are not observed using **L** alone and are attributed to the presence of the transition metal ions. Further observations, by cell-free studies, suggested that the complexes, but not the ligand, could be characterized by a bi-functional behaviour against free-DNA starting from reversible structural alterations (at low concentrations) to degradation (at high concentrations). The [**L**MCl_2] complexes behave differently from *cis*-platinum; this could be attributed to several factors such as the coordination of M^{II} by thioether S atoms, the macrocyclic

skeleton of **L** and the presence of the PPD as intercalating fragment. The molecular peculiarities exerted against free DNA, together with the biological activities monitored against a neoplastic cellular model, make both Pt^{II} and Pd^{II} complexes attractive to be further investigated in order to develop in the next future compounds with antineoplastic potential.

Abbreviations

AGE	agarose gel electrophoresis
Et-Br	ethidium bromide
PG	picogreen
PPD	2,5-diphenyl[1,3,4]oxadiazole.
DMF	Dimethylformamide
Tris	Tris(hydroxymethyl)aminomethane

Acknowledgment

We acknowledge financial support from Department of Pure and Applied Sciences, University of Urbino, LILT (Lega Italiana per la Lotta contro i Tumori) and ASSO (Associazione a Sostegno degli Studi Oncologici). CRIST (Centro di Cristallografia Strutturale, University of Firenze, Italy) where single-crystal X-ray data were collected is also thanked. S. Amatori was supported by a Fondazione Umberto Veronesi Fellowship.

Supplementary data. NMR spectra; cell viability, cell cycles and electrophoretic mobility of circular plasmid DNA. Supplementary data associated with this article can be found in the online

version. Crystallographic information files for [**L**$PdCl_2$] and [**L**$PtCl_2$]·0.5(DMF) are also available from the Cambridge Crystallographic Data Center (CCDC) upon request (http://www.ccdc.cam.ac.uk, CCDC deposition numbers 1403514 and 1403515**)**

References

[1] J. Ferlay, I. Soerjomataram, R. Dikshit, S. Eser, C. Mathers, M. Rebelo, D.M. Parkin, D. Forman, F. Bray, Int. J. Cancer 136 (2015) E359–E386.

[2] A.R. Kapdi, I.J.S. Fairlamb, Chem. Soc. Rev. 43 (2014) 4751–4777.

[3] de A. Almeida, B.L. Oliveira, J.D.G. Correia, G. Soveral, A. Casini, Coord. Chem. Rev. 257 (2013) 2689–2704.

[4] J.J. Wilson, S.J. Lippard, Chem. Rev. 114 (2014) 4470–4495.

[5] T.R. deBoer-Maggard, P.K. Mascharak, in: T. Storr (Ed.), Ligand Design in Medicinal Inorganic Chemistry, John Wiley & Sons Ltd, United Kingdom, 2014, pp. 355–374.

[6] N.P.E. Barry, P.J. Sadler, Pure Appl. Chem. 86 (2014) 1897–1910.

[7] C.-H. Leung, S. Lin, H.-J. Zhong, D.-L. Ma, Chem. Sci. 6 (2015) 871–884.

[8] M. Ashfaq, T. Najam, S.S.A. Shah, M.M. Ahmad, S. Shaheen, R. Tabassum, G. Rivera, Curr. Med. Chem. 21 (2014) 3081–3094.

[9] B. Rosenberg, L. VanCamp, J.E. Trosko, V.H. Mansour, Nature 222 (1969) 385–386.

[10] N. Farrell, in: Comprehensive Coordination Chemistry II, vol. 9, Elsevier Amsterdam, 2003, pp. 809–840.

[11] T. Boulikas, Cancer Ther. 5 (2007) 351–376.

[12] W.M. Motswainyana, M.O. Onani, A.M. Madiehe, M. Saibub, N. Thovhogi, R.A. Lalancette, Inorg. Biochem. 129 (2013) 112–118.

[13] S. Medici, M. Peana, V.M. Nurchi, J.I. Lachowicz, G. Crisponi, M.A. Zoroddu, Coord. Chem. Rev. 284 (2015) 329–350.

[14] Ž.D.Bugarčić, J. Bogojeski, R. VanEldik, Coord. Chem. Rev. 292 (2015) 91–106.

[15] N.A. Lewis, F. Liu, L. Seymour, A. Magnusen, T.R. Erves, J.F. Arca, F.A. Beckford, R. Venkatraman, A. González-Sarrías, F.R. Fronczek, D.G. VanDerveer, N.P. Seeram, A. Liu, W.L. Jarrett, A.A. Holder, Eur. J. Inorg. Chem. 4 (2012) 664–677.

[16] E. Ramachandran, P. Kalaivani, R. Prabhakaran, N.P. Rath, S. Brinda, P. Poornima, V.V. Padma, K. Natarajan, Metallomics 4 (2012) 218–227.

[17] B. Atasever, B. Ülküseven, T. Bal-Demirci, S. Erdem-Kuruca, Z. Solakoğlu, Invest. New Drugs 28 (2010) 421–432.

[18] M.X. Li, C.L. Chen, D. Zhang, J.Y. Niu, B.S. Ji, Eur. J. Med. Chem. 45 (2010) 3169–3177.

[19] V. Vrdoljak, I. Đilović, M. Rubčić, S.K. Pavelić, M. Kralj, D. Matković-Čalogović, I. Piantanida, P. Novak, A. Rožman, M. Cindrić, Eur. J. Med. Chem. 45 (2010) 38–48.

[20] K.S.O. Ferraz, L. Ferandes, D. Carrilho, M.C.X. Pinto, M.F. Leite, E.M. Souza–Fagundes, N.L. Speziali, I.C. Mendes, H. Beraldo, Bioorg. Med. Chem. 17 (2009) 7138–7144.

[21] E. Ramachandran, D.S. Raja, N.P. Rath, K. Natarajan, Inorg. Chem. 52 (2013) 1504–1514.

[22] W. Hernández, J. Paz, F. Carrasco, A. Vaisberg, E. Spodine, J. Manzur, L. Hennig, J. Sieler, S. Blaurock, L. Beyer, Bioinorg. Chem. Appl. (2013) ID524701

[23] R. Prabhakaran, P. Kalaivani, P. Poornima, F. Dallemer, R. Huang, V. Vijaya Padma, K. Natarajan, Bioorg. Med. Chem. 21 (2013) 6742–6752.

[24] M. Jamshidi, R. Yousefi, S.M. Nabavizadeh, M. Rashidi, M.G. Haghighi, A. Niazi, A. Moosavi-Movahedi, Int. J. Biol. Macromol. 66 (2014) 86–96.

[25] C. Icsel, V.T. Yilmaz, A. Golcu, E. Ulukaya, O. Buyukgungor, Bioorg. Med. Chem. Lett. 23 (2013) 2117–2122.

[26] S. Banerjee, J.A. Kitchen, S.A. Bright, J.E. O'Brien, D.C. Williams, J.M. Kelly, T. Gunnlaugsson, Chem. Commun. 49 (2013) 8522–8524.

[27] F. Ari, B. Cevatemre, E.I.I. Armutak, N. Aztopal, V.T. Yilmaz, E. Ulukaya, Bioorg. Med. Chem. 22 (2014) 4948–4954.

[28] R. Mohammadi, R. Yousefi, M.D. Aseman, S.M. Nabavizadeh, M. Rashidi, Anticancer Agents Med. Chem. 15 (2015) 107–114.

[29] P.J. Bond, R. Langridge, K.W. Jennette, S.J. Lippard, Proc. Natl. Acad. Sci. U. S. A. 72 (1975) 4825–4829.

[30] K.B. Garbutcheon-Singh, P. Leverett, S. Myersa, J.R. Aldrich-Wright, Dalton Trans. 42 (2013) 918–926.

[31] E. Gao, H. Fu, M. Zhu, C. Ma, S. Liang, J. Zhang, L. Li, L. Wang, Y. Li, W. Jiao, Eur. J. Med. Chem. 82 (2014) 172–180.

[32] D.A.K. Vezzu, Q. Lu, Y. Chen, S. Huo, J. Inorg. Biochem. 134 (2014) 49–56.

[33] Y. Sun, D. Sun, W. Yu, M. Zhu, F. Ding, Y. Liu, E. Gao, S. Wang, G. Xiong, I. Dragutan, V. Dragutan, Dalton Trans. 42 (2013) 3957–3967.

[34] Q. Qin, Z. Chen, J. Qin, X. He, Y. Li, Y. Liu, K. Huang, H. Liang, Eur. J. Med. Chem. 92 (2015) 302–313.

[35] P. Vranec, I. Potočňák, D. Sabolová, V. Farkasová, Z. Ipóthová, J. Pisarčíková, H. Paulíková, J. Inorg. Biochem. 131 (2014) 37–46.

[36] E. Gabano, S. Gama, F. Mendes, M.B. Gariboldi, E. Monti, S. Bombard, S. Bianco, M. Ravera, J. Biol. Inorg. Chem. 18 (2013) 791–801.

[37] C. Asche, Mini-Rev. Med. Chem. 5 (2005) 449-467.

[38] K. Duskova, S. Sierra, M.J. Fernández, L. Gude, A. Lorente, Bioorg. Med. Chem. 20 (2012) 7112–7118.

[39] G. Ambrosi, E. Borgogelli, M. Formica, V. Fusi, L. Giorgi, M. Micheloni, E. Rampazzo, M. Sgarzi, N. Zaccheroni, L. Prodi, Sens. Actuators B 207 (2015) 1035–1044.

[40] Agilent Technologies, Version 1.171.36.28 (release 01-02-2013 CrysAlis171 .NET; compiled Feb 1 2013,16:14:44)

[41] A. Altomare, G.L. Cascarano, C. Giacovazzo, A. Guagliardi, M.C. Burla, G. Polidori, M. Camalli, J. Appl. Cryst. 32 (1999) 115–119.

[42] G.M. Sheldrick, Acta Cryst. A64 (2008) 112–122.

[43] M. Nardelli, J. Appl. Cryst. 28 (1995) 659.

[44] C.F. Macrae, P.R. Edgington, P. McCabe, E. Pidcock, G.P. Shields, R. Taylor, M. Towler, J. van de Streek, J. Appl. Cryst. 39 (2006) 453–457.

[45] L.J. Farrugia, J. Appl. Cryst. 45 (2012) 849–854.

[46] S. Caprodossi, M. Pedinotti, C. Amantini, G. Santoni, S. Minucci, P.G. Pelicci, M. Fanelli, Mol. Biotechnol. 30 (2005) 231–238.

[47] T.C. Chou, Pharmacol. Rev. 58 (2006) 621–681.

[48] S. Amatori, F. Papalini, R. Lazzarini, B. Donati, I. Bagaloni, M.R. Rippo, A. Procopio, P.G. Pelicci, A. Catalano, M. Fanelli, Lung Cancer 66 (2009) 184–190.

[49] A. Bencini, A. Bianchi, V. Fusi, C. Giorgi, P. Paoletti, J.A. Ramirez, B. Valtancoli, Inorg. Chem. 38 (1999) 2064–2070.

[50] M. Arca, C. Caltagirone, G. De Filippo, M. Formica, V. Fusi, L. Giorgi, V. Lippolis, L. Prodi, E. Rampazzo, M.A. Scorciapino, M. Sgarzi, N. Zaccheroni, Chem. Comm. 50 (2014) 15259–15262.

[51] S.N. Dmitrieva, N.I. Sidorenko, N.A. Kurchavov, A.I. Vedernikov, A.Y. Freidzon, L.G. Kuz'mina, A.K. Buryak, T.M. Buslaeva, A.A. Bagatur'yants, Y.A. Strelenko, J.A. Howard, S.P. Gromov, Inorg. Chem. 50 (2011) 7500–7510 and references herein.

[52] F.H. Allen, Acta Cryst. B58 (2002) 380–388.

[53] C.A. Rabik, M.E. Dolan, Cancer Treat. Rev. 33 (2007) 9–23.

[54] F. Emmerling, I. Orgzall, G. Reck, B.W. Schulz, S. Stockhause, B. Schulz, J. Mol. Struc. 800 (2006) 74–84.

[55] G. Ambrosi, M. Formica, V. Fusi, L. Giorgi, E. Macedi, M. Micheloni, P. Paoli, R. Pontellini, P. Rossi, Inorg. Chem. 49 (2010) 9940–9948.

[56] S. Amatori, I. Bagaloni, E. Macedi, M. Formica, L. Giorgi, V. Fusi, M. Fanelli, Br. J. Cancer 103 (2010) 239–248.

Table 1. Selected bond distances (Å) and bond angles (°) for [**L**$PdCl_2$] and [**L**$PtCl_2$]·0.5(DMF).

	[**L**$PdCl_2$]	[**L**$PtCl_2$]·0.5(DMF)
Bond distances		
M(II)-S(1)	2.2524(7)	2.248(2)
M(II)-S(2)	2.2585(7)	2.248(2)
M(II)-Cl(1)	2.3147(7)	2.327(2)
M(II)-Cl(2)	2.3212(6)	2.310(2)
Bond angles		
S(1)-M(II)-S(2)	87.72(2)	88.82(5)
S(1)-M(II)-Cl(1)	174.03(3)	177.39(6)
S(1)-M(II)-Cl(2)	86.86(2)	88.26(6)
S(2)-M(II)-Cl(1)	92.33(3)	91.91(5)
S(1)-M(II)-Cl(2)	171.90(3)	176.60(6)
Cl(1)-M(II)-Cl(2)	93.69(2)	91.08(6)

Table 2. Crystallographic and refinement details for for [**L**$PdCl_2$] and [**L**$PtCl_2$]·0.5(DMF).

	[**L**$PdCl_2$]	[**L**$PtCl_2$]·0.5(DMF)
Empirical formula	$C_{24}H_{30}Cl_2N_4OPdS_2$	$C_{25.5}H_{34.5}Cl_2N_{4.5}O_{1.5}PtS_2$
Formula weight	631.94	758.18
Temperature (K)	150	120
Wavelength (Å)	0.71073	0.71073
Crystal system, space group	Triclinic, P-1	Triclinic, P-1
Unit cell dimensions (Å, °)	a = 9.3458(3), α = 113.315(4)	a = 9.2032(6), α = 65.576(5)
	b = 11.8259(5), β= 92.162(3)	b = 12.7351, β= 88.176(5)
	c = 13.5850(7), γ = 106.011(3)	c = 13.1310(8), γ = 83.832(4)
Volume ($Å^3$)	1306.9(1)	1393.0(2)
Z, Dc (mg/cm^3)	2, 1.606	2, 1.808
μ(mm^{-1})	1.100	5.409
F(000)	644	750
Crystal size (mm)	0.36x0.28x0.25	0.42x0.30x0.28
θ range (°)	4.20 to 32.46	4.11 to 29.46
Reflections collected / unique	19905 / 8336	21183 / 6586
Data / parameters	8336 / 397	6586 / 349
Goodness-of-fit on F^2	1.054	1.029
Final R indices [I>2σ(I)]	R1 = 0.0405, wR2 = 0.0769	R1 = 0.0499, wR2 = 0.0906
R indices (all data)	R1 = 0.0636, wR2 = 0.0896	R1 = 0.0718, wR2 = 0.1039

Captions to schemes and figures

Scheme 1. Possible conformations adopted by the the 2,5-diphenyl[1,3,4]oxadiazole (PPD) (top); molecular fragments searched in the Cambridge Structural Database (bottom).

Figure 1. Ligand **L** with atom labelling used in NMR assignments.

Figure 2. ^{1}H NMR spectra of **L**, [**L**$PdCl_2$] and [**L**$PtCl_2$] species in DMF-d_7 at 298 K.

Figure 3. Ortep-3 view of complexes [**L**$PdCl_2$] (top) and [**L**$PtCl_2$] (bottom). For the sake of clarity hydrogen atoms are not shown; ellipsoid probability = 30%.

Figure 4. Molecular overlay of the X-ray structures of [**L**$PdCl_2$] (stick) and [**L**$PtCl_2$] (ball and stick).

Figure 5. Fluorimetric assay**.** Dose-dependent inhibition of DNA staining by the indicated compounds. Values are reported as mean ± SD of five independent experiments. Cis-Pt, cisplatin.

Figure 6. DNA electrophoretic mobility assay. Effects on the migration of supercoiled (white arrow) and open circular (black arrow) forms of plasmid DNA (pLL3.7) by the indicated compounds. NT, not treated; C, DMF.

Figure 7. DNA electrophoretic mobility assay. Effects on the migration of linearized form of pLL3.7 plasmid DNA (black arrow) by the indicated compounds. NT, not treated; C, DMF.

Figure 8. Dose-dependent activity of the indicated compounds on U937 promonocytic leukemia cells viability measured by trypan blue dye exclusion assay**.** Values are reported as mean ± SD of three independent experiments. Cis-Pt, cisplatin.

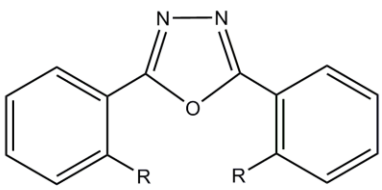

cisoid I

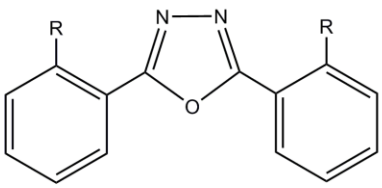

cisoid II

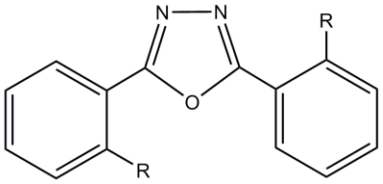

transoid

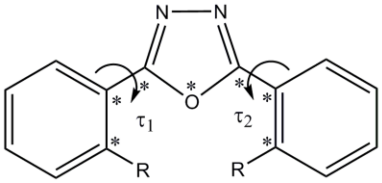

Scheme 1.

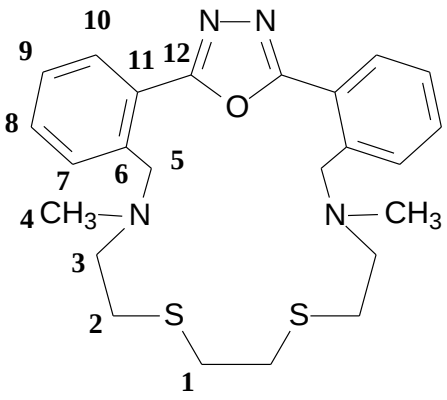

Figure 1.

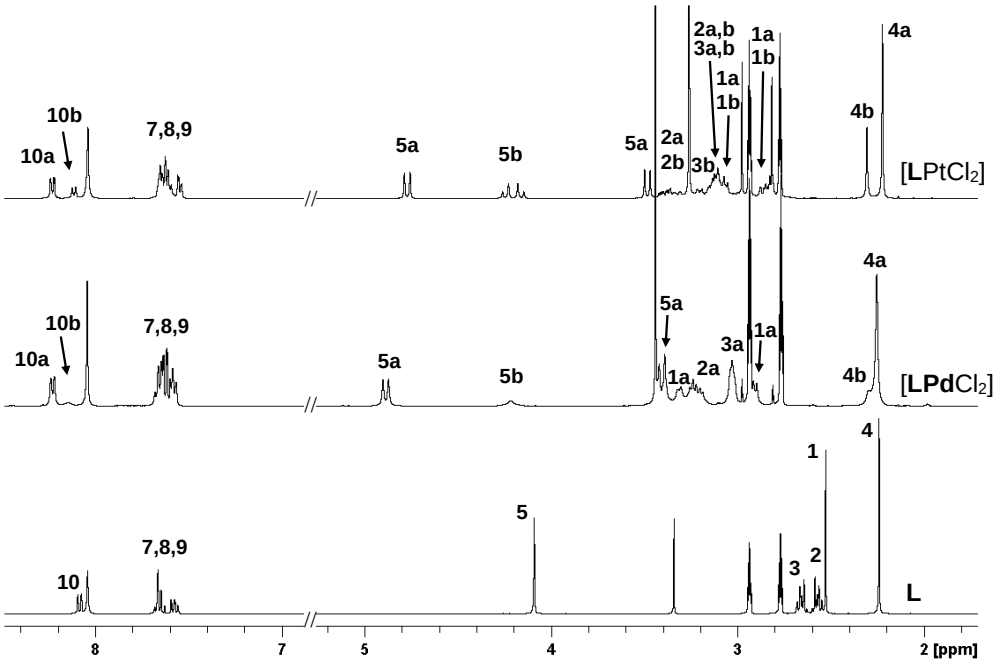
10b
10a
7,8,9
5a
5b
5a
2a,b
3a,b
1a
1b
2a
2b
3b
1a
1b
4b
4a
[LPtCl2]
4a
10b
10a
7,8,9
5a
5b
5a
1a
2a
3a
1a
4b
[LPdCl2]
4
1
5
7,8,9
10
3
2
L
8
7
5
4
3
2 [ppm]

Figure 2.

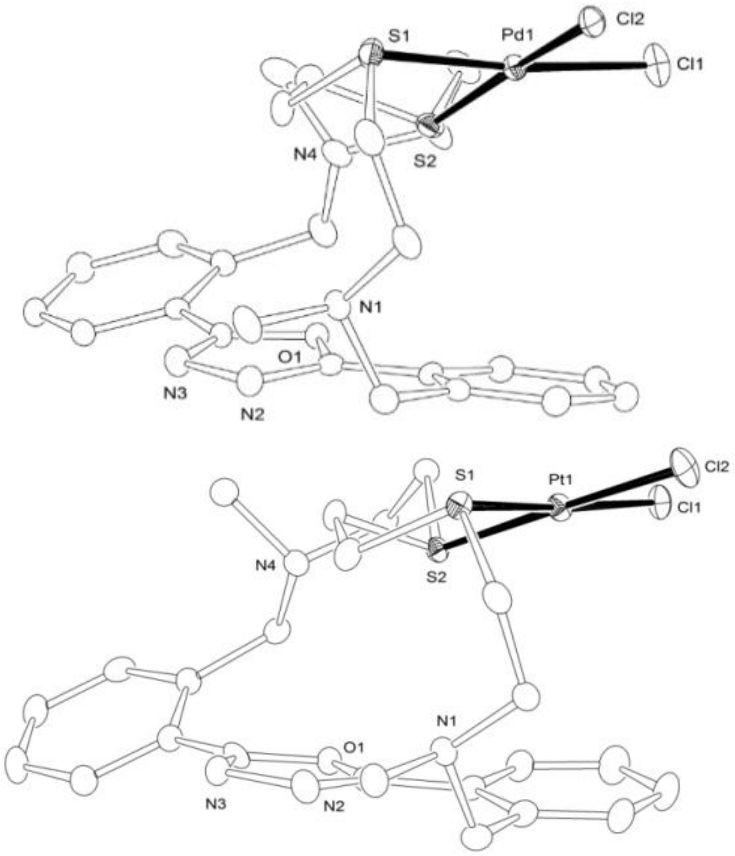

Figure 3.

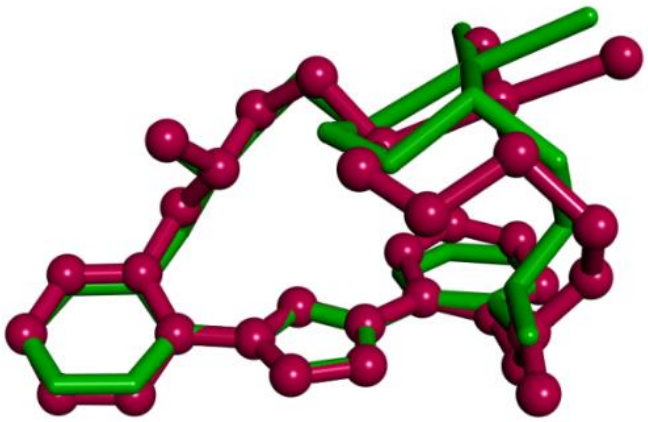

Figure 4.

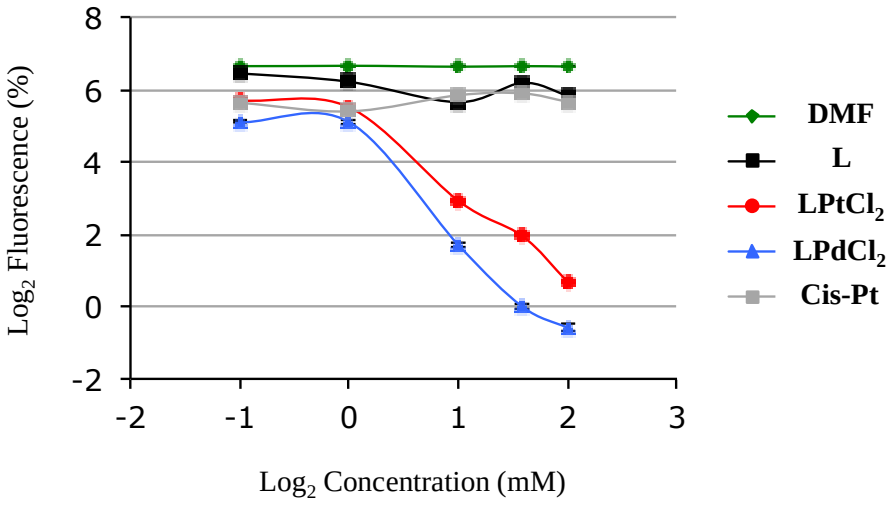
8
6
4
2
0
-2
-2
-1
0
1
2
3
Log2 Fluorescence (%)
Log2 Concentration (mM)
DMF
L
LPtCl2
LPdCl2
Cis-Pt

Figure 5.

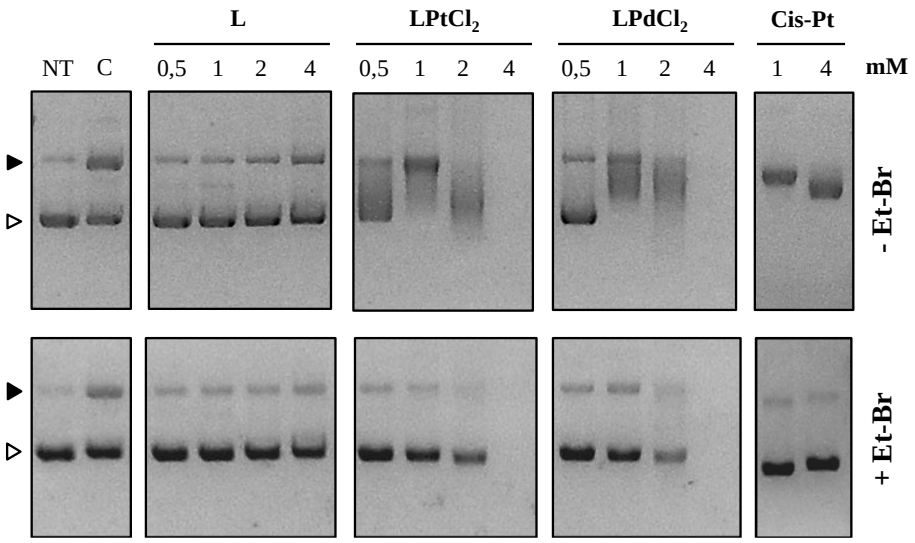

Figure 6.

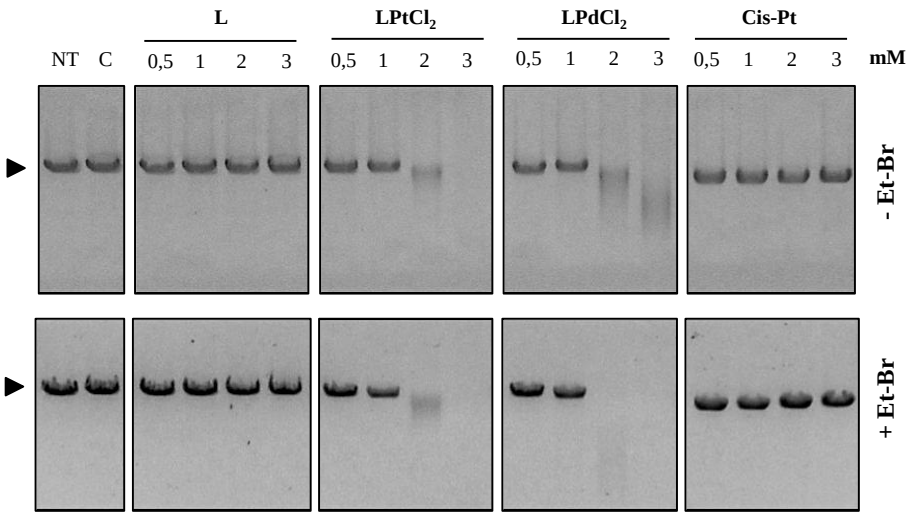
L
LPtCl2
LPdCl2
Cis-Pt
NT C 0,5 1 2 3 0,5 1 2 3 0,5 1 2 3 0,5 1 2 3 mM
- Et-Br
+ Et-Br

Figure 7

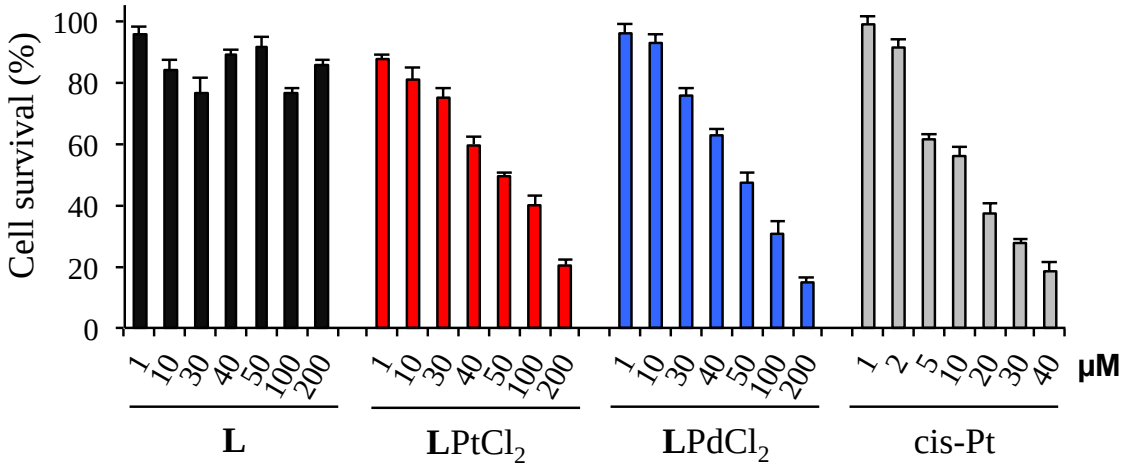
Cell survival (%)
100
80
60
40
20
0
1 10 30 40 50 100 200
1 10 30 40 50 100 200
1 10 30 40 50 100 200
1 2 5 10 20 30 40
μM
L
LPtCl2
LPdCl2
cis-Pt

Figure 8.